ACS APPLIED MATERIALS & INTERFACES

www.acsami.org

Research Article

Low-Temperature Direct Growth of Amorphous Boron Nitride Films for High-Performance Nanoelectronic Device Applications

Seyed Mehdi Sattari-Esfahlan, Hyoung Gyun Kim, Sang Hwa Hyun, Jun-Hui Choi, Hyun Sik Hwang, Eui-Tae Kim, Hyeong Gi Park,* and Jae-Hyun Lee*

Cite This: *ACS Appl. Mater. Interfaces* 2023, 15, 7274–7281

Read Online

ACCESS | Metrics & More | Article Recommendations | Supporting Information

ABSTRACT: We successfully demonstrated the improvement and stabilization of the electrical properties of a graphene field effect transistor by fabricating a sandwiched amorphous boron nitride (a-BN)/graphene (Gr)/a-BN using a directly grown a-BN film. The a-BN film was grown *via* low-pressure chemical vapor deposition (LPCVD) at a low growth temperature of 250 °C and applied as a protection layer in the sandwiched structure. Both structural and chemical states of the as-grown a-BN were verified by various spectroscopic and microscopic analyses. We analyzed the Raman spectra of Gr/SiO_2 and a-BN/Gr/a-BN structures to determine the stability of the device under exposure to ambient air. Following exposure, the intensity of the 2D/G-peak ratio of Gr/SiO_2 decreased and the position of the G and 2D peaks red-shifted due to the degradation of graphene. In contrast, the peak position of encapsulated graphene is almost unchanged. We also confirmed that the mobility of a-BN/Gr/a-BN structure is 17,941 cm^2/Vs. This synthetic strategy could provide a facile way to synthesize uniform a-BN film for encapsulating various van der Waals materials, which is beneficial for future applications in nanoelectronics.

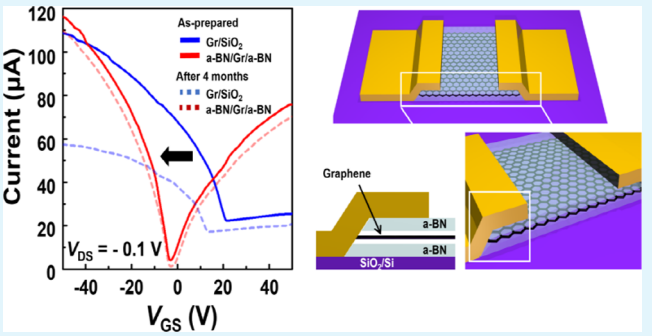

KEYWORDS: *amorphous boron nitride (a-BN), graphene, heterojunction, field effect transistor (FET), high mobility, boron nitride encapsulation*

INTRODUCTION

Graphene has been widely used in a variety of applications, such as in field effect transistors (FETs) and memory and tunneling devices, because of its superior electrical properties.[1−6] However, graphene has a limitation in that all its carbon atoms are exposed to the external environment, which could cause performance degradation of graphene-based devices.[7−9] After exposure to the external environment, silanol groups on the SiO_2 surface interfere with the movement of charge carriers, resulting in localized charge accumulation at the interface between graphene and SiO_2.[10−12] Numerous approaches have been introduced to enhance the stability and performance of graphene-based devices.[13−15] Encapsulating such devices using various 2D materials (2DMs) can prevent their deterioration due to external effects.[16−21] In particular, hexagonal boron nitride (h-BN) films have many advantageous properties such as a large band gap of approximately 6 eV, and a dielectric constant of ∼3.76. h-BN films have the same hexagonal atomic structure and high crystallinity as 2DMs; thus, they can improve mobility and stabilize device performance (Table S1).[18−21] Several research groups have demonstrated the large-scale growth of h-BN on metal catalytic substrates;[22−24] however, because of the wet-etching process of metal catalysts during stacking with other 2DMs, contamination at the interface is inevitable.[25] In addition, to obtain an h-BN film with a large area, a high growth temperature and a long growth time are required. As an alternative for the crystalized h-BN, amorphous boron nitride (a-BN) has been considered a promising encapsulating material for 2DMs because it is relatively free of defects (traps and dangling bonds) and requires low growth temperature.[26−31] Glavin et al. and Hong et al. explored the dielectric properties of ultrathin a-BN film and diffusion barrier behavior for ultrathin electronic devices.[28,29] Uddin et al. confirmed that FETs of graphene on an a-BN heterointerface could enhance the hole and electron mobilities to 4980 and 4200 cm^2/Vs, respectively.[30] Very recently, Lu et al. verified that a-BN film successfully suppresses current fluctuations and enhances carrier mobility of 2D materials.[31] However, fabricating a-BN films still has several issues, such as the requirement of additional annealing processes at relatively high temperatures, complicated processes for making the protection layer, and the debate over

Received: October 18, 2022
Accepted: January 12, 2023
Published: January 31, 2023

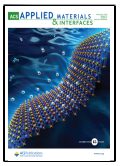

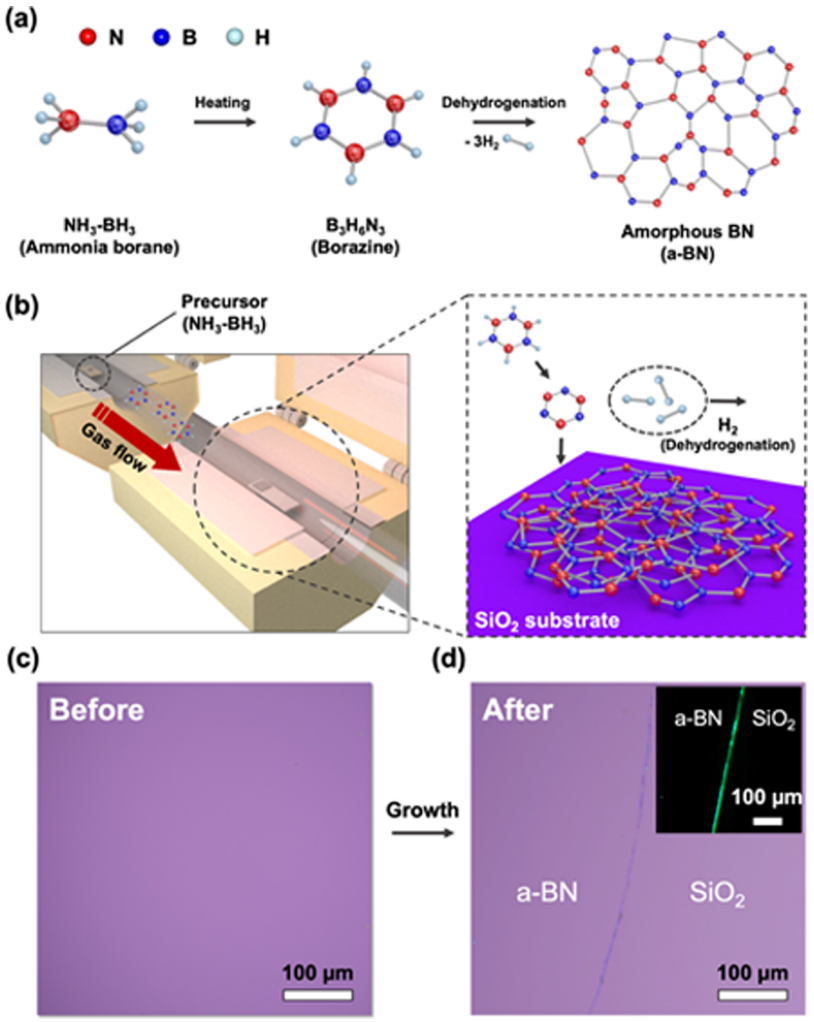

Figure 1. Schematic illustration of the (a) growth mechanism of the a-BN film and (b) double-zone low-pressure chemical vapor deposition system. The solid-phase precursor vaporizes in furnace 1 and is supplied into furnace 2. Optical microscopic (OM) images of 300 nm SiO_2/Si substrates (c) before and (d) after a-BN growth. (Inset) Dark-field OM image apparently shows the synthesized a-BN on 300 nm SiO_2/Si.

the transfer process. Above all, experiments to confirm whether a-BN can sufficiently protect 2D materials from the external environment and help improve electrical performance have not been appropriately explored or performed yet (Table S2).

In this study, we succeeded in growing centimeter-sized uniform a-BN films on arbitrary substrates (e.g., graphene/Ge substrate and SiO_2/Si substrate) at a low temperature. Using X-ray photoemission spectroscopy (XPS), Raman spectroscopy, and high-resolution transmission electron microscopy (HR-TEM), we verified the high disorderness and near-stoichiometry of the BN film. A capacitance−voltage ($C-V$) analysis was performed to evaluate the electrical properties of the as-grown a-BN film, and the dielectric constant of a-BN was approximately 1.25 at 1 MHz, very close to the κ of air. Since the a-BN film could be directly grown on the graphene/Ge substrate, we assembled a-BN/graphene/a-BN heterostructure without a wet-etching transfer process. Notably, we fabricated FET-based a-BN-encapsulated graphene and confirmed the enhancement of both stability and transport properties, even after 4-month of exposure to ambient air conditions.

EXPERIMENTAL DETAILS

Low-Temperature Growth of a-BN on an Arbitrary Substrate. a-BN films were synthesized using a 2-inch double-zone low-pressure chemical vapor deposition system, which was divided into a precursor-vaporization zone (furnace 1) and a reaction zone (furnace 2) (Figure 1). First, ammonia−borane complex (NH_3-BH_3, 97% purity, 10 mg, Sigma-Aldrich) powder and arbitrary substrates of 1.5 × 1.5 cm^2 size (graphene/Ge substrate or 300 nm SiO_2/Si substrate) were loaded into furnaces 1 and 2, respectively. The detailed protocol for the growth of graphene on the Ge substrate is described in Figure S1 in the Supplementary Information.[32] The chamber was evacuated to a high vacuum (~1 mTorr) for 30 min. Then, furnace 2 was heated to 250 °C while maintaining 110 Torr at a flow of 20 sccm of H_2 (99.999%) and furnace 1 was heated to 100 °C for 30 min to form dehydrogenated $B_3N_6H_3$ molecules. Simultaneously, evaporated $B_3N_6H_3$ molecules begin to deposit on the substrate in furnace 2 (Figure 1b). After obtaining the a-BN film of the desired thickness, both furnaces were cooled to room temperature to avoid further growth. Figure 1c,d shows OM images of a 300 nm SiO_2/Si substrate before and after a-BN growth, which indicates that the as-grown a-BN is uniform and transparent (surface morphology and average thickness of a-BN is described in Figure S2).[27]

Encapsulation and Device Fabrication. Both encapsulation and device fabrication processes are schematically described in Figure S3a. We deposited a 40 nm Au film on an a-BN film-coated graphene/Ge substrate (a-BN/Gr/Ge) through thermal evaporation. Then, poly(methyl methacrylate) (PMMA) solution (PMMA A4, 4% by weight of PMMA in anisole) was spin-coated on the samples at 2500 rpm for 60 s and samples were baked at 120 °C for 10 min. Consequently, a thermal

https://doi.org/10.1021/acsami.2c18706
ACS Appl. Mater. Interfaces 2023, 15, 7274−7281

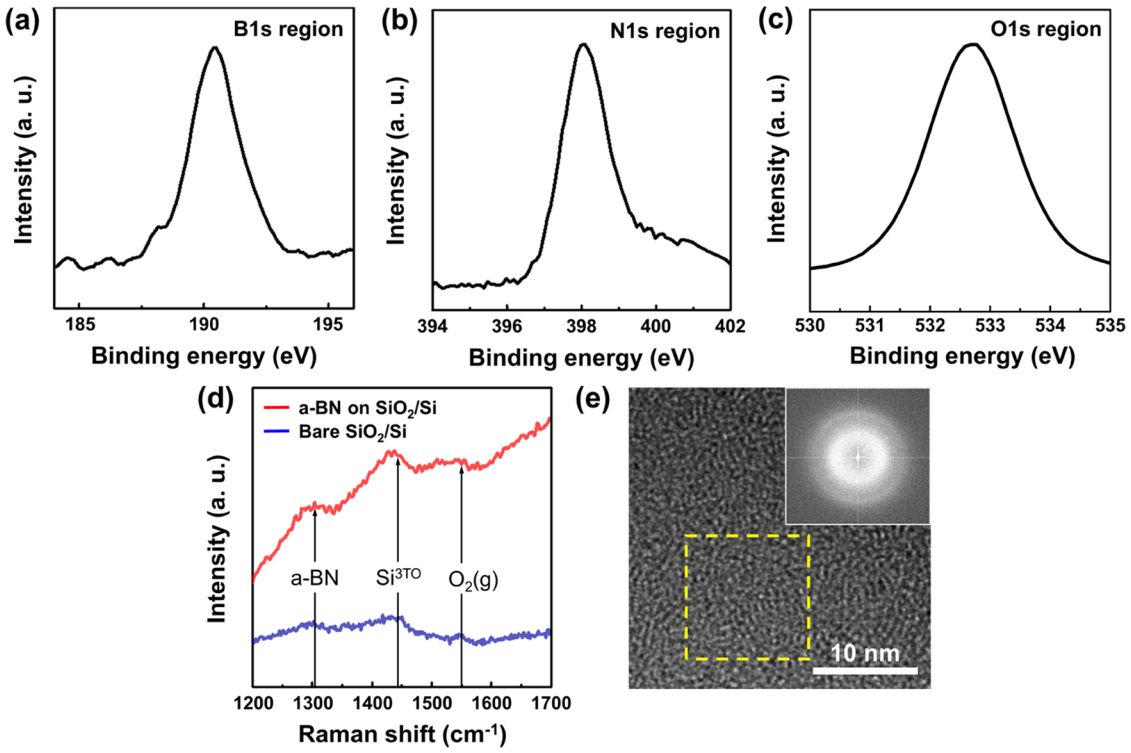

Figure 2. (a–c) N 1s, B 1s, and O 1s region in XPS profiles for the a-BN film on a 300 nm SiO_2/Si substrate. (d) Raman spectra acquired from the as-grown a-BN film on a 300 nm SiO_2/Si substrate (red) and bare 300 nm SiO_2/Si substrate (blue). (e) HR-TEM image of the a-BN film. The inset image shows a fast Fourier transform results of the area depicted in the yellow box inside Figure 2e, indicating a disordered arrangement.

release tape (TRT) was attached, and a mechanical exfoliation method was used to separate a-BN/Gr from the Ge substrate. The stacked TRT/PMMA/Au film/a-BN/Gr structure was transferred onto an a-BN/SiO_2/Si substrate using a thermal press at 100 °C for 5 min. After detaching TRT at 120 °C, PMMA was removed using hot (50 °C) acetone treatment for 1 h and dipping in isopropyl alcohol to remove any residual PMMA. The Au film was removed using potassium iodide/iodine (KI/I_2) solution. The two-terminal device structure was patterned by standard photolithography (width: 2.0 μm and length: 3.0 μm). To expose the graphene edge, patterned a-BN regions were etched away using plasma etching (a mixture of 10 sccm of Ar and SF_6 at 100 W for 2 min). A thermal evaporator was used to deposit 15 nm Cr and 85 nm Au metals as metal electrodes for the source and drain of the FET devices. To compare the performance of the device, we prepared a graphene-based FET device on a 300 nm SiO_2/Si substrate (Figure S3b).

Characterization. HR-TEM analysis was performed using a Seron AIF 2100 (Philips CM30). Film thickness was characterized by HR-TEM and atomic force microscopy (AFM, scan rate: 0.5 Hz, Park NX10, Park System). Raman spectroscopy (Alpha300 M+, WITec GmbH) with an excitation wavelength of 532 nm and a Nd:YLF laser was used to investigate the crystal properties of the samples (graphene and a-BN film for a laser power of 5 and 30 mW, respectively). The chemical composition of amorphous boron nitride and graphene were determined by XPS using an ESCA2000 spectrometer; a-BN (power = 120 W, calibration peak: C 1s with a peak at around 284.8 eV) and graphene (power = 80 W, calibration peak: C 1s with a peak at about 284.6 eV). A Keithley 2400 was used to measure the $I-V$ characteristics of both types of graphene FET devices at room temperature (compliance: 0.01 A and scan step: 0.1 V). The capacitance–voltage ($C-V$) characteristics of the Ag/a-BN/Si/Ag configuration were measured using a K4200A-SCS parameter analyzer system and a probe station facility at room temperature under ambient conditions. The top and bottom electrodes with thicknesses of 100 nm were deposited on a-BN and Si.

RESULTS AND DISCUSSION

Chemical and Electrical Properties of the a-BN Film. The elemental composition of the a-BN film was analyzed by XPS. High-resolution XPS scans of the B 1s and N 1s depicted single distributed boron and nitrogen atomic bonds, with peaks at 190.4 and 398.1 eV, respectively (Figure 2a,b).[29] The peak locations and lack of secondary peaks indicate very low levels of impurities in the a-BN film. Surface oxidation can hinder the encapsulation of the a-BN layer and is commonly reported in BN films.[33] However, oxidation peaks (around 192.1 eV) were absent in the XPS spectrum, indicating that the a-BN thin film surface was not oxidized. Figure 2b shows almost no fingerprint of metallic B–B bonding, which appears at B 1s ≈ 187 eV. Additionally, the ratio of B to N was nearly 1 to 1, demonstrating stoichiometric a-BN thin film growth. As shown in Figure 2c, the O 1s peak was observed at 532.7 eV, originating from the bottom SiO_2/Si substrate. Compared to the O 1s peak of bare SiO_2/Si substrate, the hydroxyl groups on the SiO_2 surface were almost eliminated during a-BN film growth, indicating that the as-grown a-BN film well passivated the hydrophilic SiO_2 surface (Figure S4).[34]

Raman spectroscopy was performed to check the noncrystalline state of the a-BN film on the SiO_2/Si substrate. As shown in Figure 2d, the a-BN samples exhibit an amorphous growth status compared to bare SiO_2/Si. Three peaks were observed from 1200 to 1700 cm^{-1} for the a-BN film. The small peak near 1300 cm^{-1} is ascribed as E_{2g} vibrational mode of BN, which has been shifted to a lower wave number from the peak position of hybridized BN with sp^2 bonds at around 1370 cm^{-1}.[35−37] This large shift might be due to the random strain effect dominating the degradation of the crystal structure.[36−38] The broad peaks at 1450 and 1550 cm^{-1} were assigned to the third-order transverse optical phonon originating from the Si substrate and the

https://doi.org/10.1021/acsami.2c18706
ACS Appl. Mater. Interfaces 2023, 15, 7274−7281

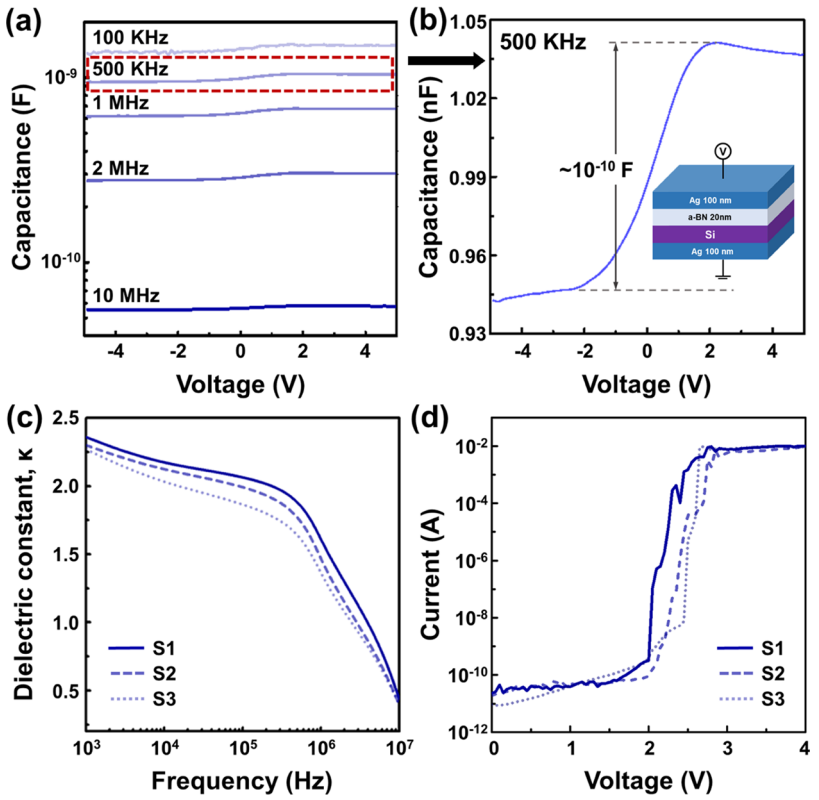

Figure 3. (a) Capacitance as a function of voltage, (b) maximized figure of capacitance changes *via* voltage, (c) relative dielectric constant versus frequency, and (d) *I*−*V* characteristics of a-BN samples.

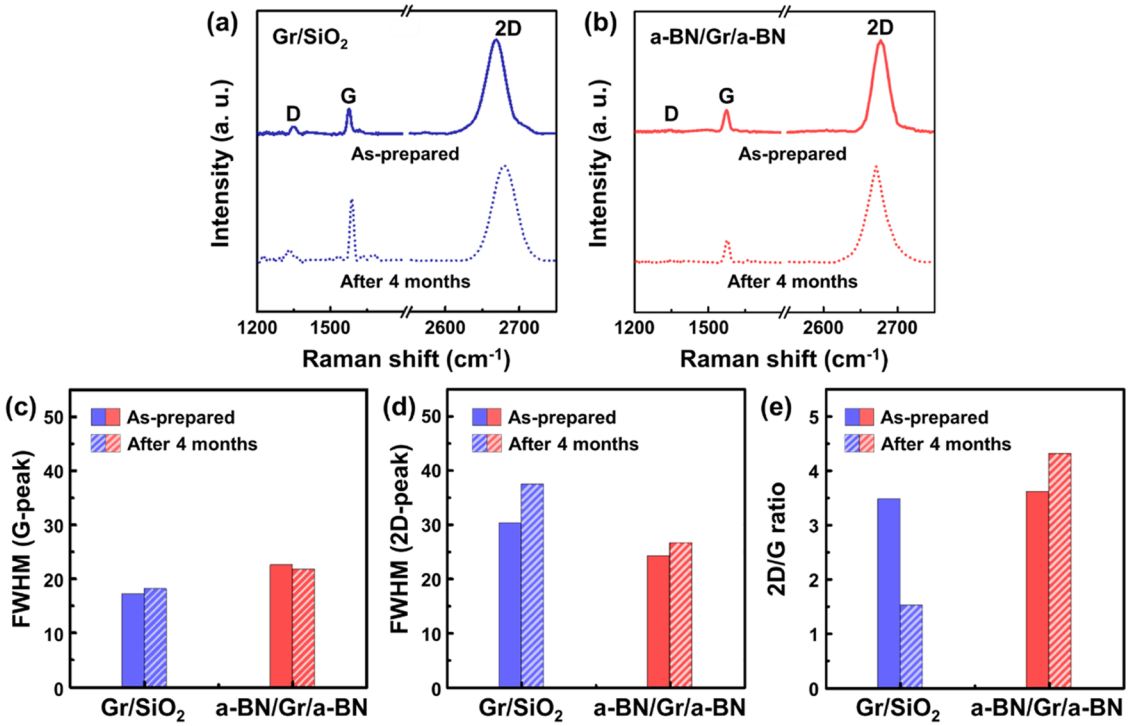

Figure 4. Raman spectra analysis for (a) Gr/SiO_2, and (b) a-BN/Gr/a-BN samples; as prepared and after 4 months. Calculated full width at half-maximum for (c) G-peak and (d) 2D-peak. (e) Value of 2D/G compared in as prepared and after 4 months.

molecular oxygen (e.g., ambient oxygen), respectively.[37,38] We analyzed the as-grown a-BN films using top-view TEM images (Figure 2e) to prove the noncrystalline structure and electron diffraction patterns of the grown BN films and found the absence of long-range atomic order (refer to the amorphous nature of BN).

To verify the electrical properties of the as-grown a-BN, we prepared three samples with the Ag/a-BN/Si/Ag configuration

https://doi.org/10.1021/acsami.2c18706
ACS Appl. Mater. Interfaces 2023, 15, 7274−7281

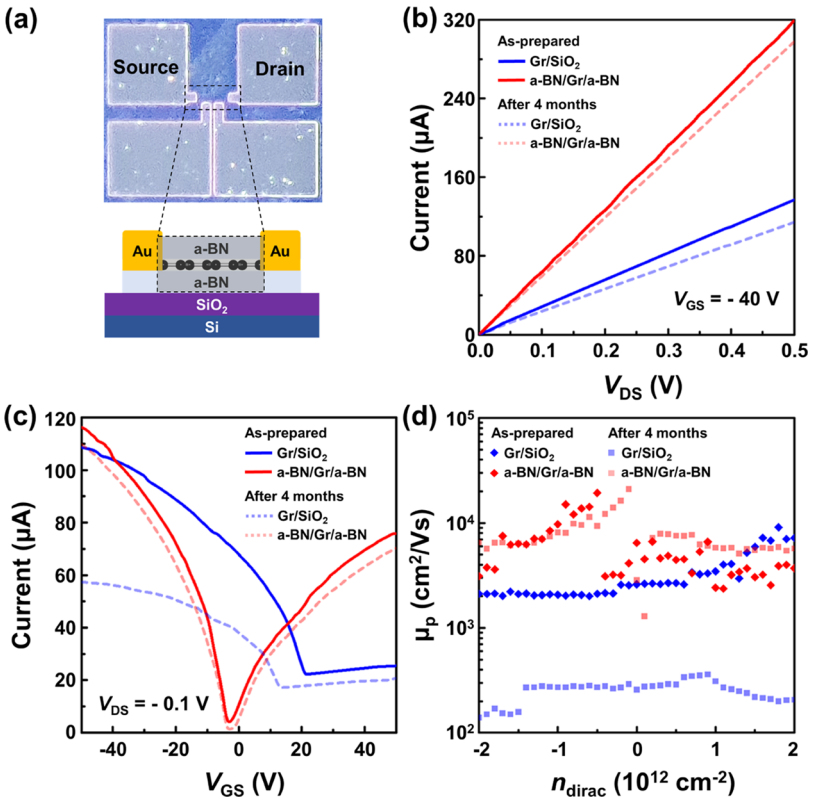

Figure 5. Optical microscope image of FET device structure of (a) Gr/SiO_2 and a-BN/Gr/a-BN, (b) drain current (I_D) with drain-source voltage (V_{DS}) curves, (c) transfer curves I_D-gate-source (V_{GS}) of two samples, (d) field effect mobility for two samples of as prepared and after 4 months.

(Figure 3). The thickness of a-BN was 20.4 nm for all samples (Figure S5). The capacitance value decreased by more than 1 order of magnitude when the applied frequency was increased from 100 kHz to 10 MHz (Figure 3a). For instance, the capacitance at 3 V was reduced from 5.8×10^{-11} to 1.48×10^{-9} F, when the frequency was increased to 10 MHz. The magnified view of capacitance shows that capacitance increases as a function of voltage (see Figure 3b) for a frequency of 500 kHz. The relative dielectric constants (κ) of a-BN at different frequencies are shown in Figure 3c. At 1 kHz, the κ value was approximately 2.3, and it decreased to approximately 0.4 at 10 MHz, which is close to the findings reported in the literature.[39,40] Significantly, the κ value for a-BN was approximately 1.25 at 1 MHz, very close to the κ of air. This low κ value is probably due to the absence of crystalline order in the a-BN structure, which hinders the dipole alignment.[19] The $I-V$ characteristics of the a-BN film are shown for the three samples in vertical electrode configurations (Figure 3d). The current increased gently up to approximately 2 V (Poole–Frenkel tunneling) and then dramatically enhanced due to leakage current flow, resulting in an electrical breakdown in the sample at approximately 2.6 V.

a-BN/Graphene/a-BN Encapsulation. Owing to its ultrathin layers, the structural morphology of graphene is severely affected by the substrate, resulting in different degrees of local structure.[41] Furthermore, it has been proven that SiO_2 substrates may facilitate the facile degradation of monolayer graphene under ambient conditions by reducing its stability against oxidation.[42] These ambient-related factors modify the transport properties, such as graphene's carrier mobility and conductance. Here, we fabricated sandwiched a-BN/Gr/a-BN structures on a SiO_2/Si substrate for the stability of the channel layer, which was then exposed to ambient air for 4 months. Figure 4a,b presents the Raman spectra of a-BN/Gr/a-BN compared to those of Gr/SiO_2 before and after exposure to ambient air. Three peaks were identified: the D-peak at approximately 1350 cm^{-1} comes from transverse optical phonons around the Brillouin zone corner K, the G-peak at approximately 1580 cm^{-1} originates from the emission of zone-center optical phonons (in-plane phonon mode), and the 2D-peak at approximately 2700 cm^{-1} corresponds to the high-energy second-order process, which was induced by preferential coupling to transverse optical phonons near the edge of the Brillouin zone.[43−45]

In the case of Gr/SiO_2 as a channel layer, both G-peak and 2D-peak were red-shifted and broadened at the same time after exposure to the ambient air: The peak position of G and 2D peaks at 1577.9 and 2669.2 cm^{-1} changed to 1588.7 and 2680.6 cm^{-1}, respectively, and the full width at half-maximum (FWHM) values of the G and 2D peaks increased from 17.1 and 30.2 cm^{-1} to 18.14 and 37.4 cm^{-1}, respectively (Figure 4c,d). A redshift is an increase in wavenumber, with a corresponding decrease in the frequency of an electromagnetic wave, which means that the frequency of phonons interacting with the incident photon decreases.[46,47] Ambient conditions and the adsorption of molecules, such as O_2, on the surface of graphene vary the chemical interactions, thus altering the peak position and width in the Raman spectrum.[48] Furthermore, we observed that the peak ratio of G and 2D peaks ratio of the Gr/SiO_2 samples decreased to 1.5 from its initial value of approximately 3.5. Thus, we believe that when the graphene is exposed to ambient air, disordering and oxidation of the graphene can occur, increasing the concentration of charged impurities in the graphene.[49−52] On the contrary, when the graphene is perfectly encapsulated by the a-BN (a-BN/Gr/a-BN

https://doi.org/10.1021/acsami.2c18706
ACS Appl. Mater. Interfaces 2023, 15, 7274−7281

structure), we confirmed that the width of the peaks has narrowed compared to those of the Gr/SiO_2 sample and there is little change in the Raman spectrum after 4 months of exposure to ambient air. Although the peak position of 2D slightly shifted by around 4 cm^{-1}, there was no change in the 2D/G ratio and FWHM values, indicating that the quality of graphene has not degraded.

Device Stability of Field Effect Transistor (FET). Figure 5a shows the top view of the optical microscope image of FET devices with a sandwiched a-BN/Gr/a-BN structure and its electrical properties based on the FET device. The I_D-V_{DS} curves of the two samples (FETs based on a-BN/Gr/a-BN and Gr/SiO_2) were evaluated. The current level of Gr/SiO_2 was 137 μA (a-BN/Gr/a-BN: 319 μA) at V_{DS} = 0.5 V. After 4 months, the current level of both a-BN/Gr/a-BN and Gr/SiO_2 samples were decreased to 114 and 297 μA, respectively. The a-BN/Gr/a-BN FET device can be operated at a significantly higher I_D than that of the graphene FET (GFET) on the SiO_2 substrate, as shown in Figure 5b. Furthermore, no hysteresis effect was observed in a-BN-encapsulated FET devices, probably because of the clean graphene/a-BN interface and the absence of adsorbed impurities on the GFET channel surface.[53] Figure 5c shows the transfer curves (I_D-V_{GS}) of the GFET devices. The results demonstrate that the device performance of the sandwiched a-BN/Gr/a-BN structure reached a positive neutrality point voltage (V_{NP}) around −2 V, which resulted in fewer charge traps. This leads to enhanced electron flow owing to the surface dielectric screening effect.[54] For the Gr/SiO_2 FET, the neutrality point voltage shifted to 12.5 V, which is mainly attributed to the dopants adsorbed on the graphene surface owing to its storage under relatively humid ambient conditions. As shown in Figure 5d, we extracted the field effect mobility (μ_{FE}) to compare the device performances of the sandwiched structure of the FET device to that of the Gr/SiO_2 structure using the following equation[55]

$$\mu_{FE} = \frac{\partial I_{DS}}{\partial V_{GS}} \times \frac{L}{WC_G V_{DS}}$$

where L, W, V_{DS}, and V_{GS} are the channel length, channel width, drain-source voltage, and gate-source voltage, respectively, and the capacitance per unit area (C) is $\varepsilon_0\varepsilon$/d, with relative permittivities of 4 and 2 for SiO_2 and a-BN, respectively. For the Gr/SiO_2 FET device (Figure 5d), the field effect mobility around the low-carrier-density regime ($n \approx 0.1 \times 10^{12}$ cm^{-2}) was approximately 698 cm^2/Vs, whereas that of a-BN-encapsulated FET was 17,941 cm^2/Vs, resulting in an approximately 26-fold enhancement in carrier mobility. We conclude that the electrical properties of the graphene channel a-BN can be effectively improved and it can be protected from degradation under external environmental exposure.

CONCLUSIONS

In summary, we successfully synthesized large-area a-BN films at a low temperature of 250 °C and performed optical, chemical, structural, and electrical analyses. Chemical analysis revealed that our a-BN film has sp^2-bonded B and N. a-BN films have been synthesized for various applications and can be used to fabricate sandwich structures via dry exfoliation transfer processes. We analyzed the a-BN film and stability of the a-BN/Gr/a-BN structure compared to the Gr/SiO_2 structure and fabricated FET devices to improve the field effect mobility. The μ_{FE} of a-BN/Gr/a-BN was better than that of Gr/SiO_2, achieving a value of 21,000 cm^2/Vs. Also, the current of the Gr/SiO_2 structured FET device was 114 μA at V_{DS} = 0.5 V, compared to 297 μA for the a-BN/Gr/a-BN structured FET device. We believe that our study of FET devices with a sandwiched a-BN/Gr/a-BN structure will be helpful for applications in future nanoelectronics based on ultrathin vdW materials.

ASSOCIATED CONTENT

Supporting Information

The Supporting Information is available free of charge at https://pubs.acs.org/doi/10.1021/acsami.2c18706.

Detailed information on the growth of single-crystal graphene on Ge substrate, thickness and uniformity of a-BN, encapsulation and device fabrication process, and the O 1s spectrum of bare SiO_2/Si substrate (PDF)

AUTHOR INFORMATION

Corresponding Authors

Hyeong Gi Park − *AI-Superconvergence KIURI Translational Research Center, Ajou University School of Medicine, Suwon 16499, Korea;* orcid.org/0000-0002-9590-1623; Email: hgpark007@ajou.ac.kr

Jae-Hyun Lee − *Department of Material Science and Engineering, Ajou University, Suwon 16499, Korea; Department of Energy Systems Research, Ajou University, Suwon 16499, Korea;* orcid.org/0000-0001-5117-8923; Email: jaehyunlee@ajou.ac.kr

Authors

Seyed Mehdi Sattari-Esfahlan − *Department of Material Science and Engineering, Ajou University, Suwon 16499, Korea; Department of Materials Science and Engineering, Seoul National University, Seoul 08826, Korea; Institute for Microelectronics, TU Wien, Vienna 1040, Austria;* orcid.org/0000-0002-4596-6015

Hyoung Gyun Kim − *Department of Materials Science and Engineering, Seoul National University, Seoul 08826, Korea*

Sang Hwa Hyun − *Department of Material Science and Engineering, Ajou University, Suwon 16499, Korea; Department of Energy Systems Research, Ajou University, Suwon 16499, Korea*

Jun-Hui Choi − *Department of Material Science and Engineering, Ajou University, Suwon 16499, Korea; Department of Energy Systems Research, Ajou University, Suwon 16499, Korea*

Hyun Sik Hwang − *Department of Material Science and Engineering, Ajou University, Suwon 16499, Korea; Department of Energy Systems Research, Ajou University, Suwon 16499, Korea*

Eui-Tae Kim − *Department of Materials Science and Engineering, Chungnam National University, Daejeon 34134, Korea;* orcid.org/0000-0002-5488-7159

Complete contact information is available at: https://pubs.acs.org/10.1021/acsami.2c18706

Notes

The authors declare no competing financial interest.

ACKNOWLEDGMENTS

This research was supported by the National Research Foundation (NRF) fund of Korea (NRF-

2021R1A2C2012649, and NRF-2021M3H1A104892211) and by the Ajou University research fund. The authors are thankful for the help of Prof. M. Kim from Seoul National University.

■ ABBREVIATIONS

a-BN, amorphous boron nitride
Gr, graphene
FET, field effect transistor
LPCVD, low-pressure chemical vapor deposition
2DMs, 2D materials
h-BN, hexagonal boron nitride
OM, optical microscope
HR-TEM, high-resolution TEM
AFM, atomic force microscopy
XPS, X-ray photoelectron spectroscopy
I−*V*, current−voltage
C−*V*, capacitance−voltage
TO, transverse optical
FWHM, full width at half-maximum
GFETs, graphene FETs
V_{NP}, neutrality point voltage
μ_{FE}, field effect mobility

■ REFERENCES

(1) Novoselov, K. S.; Fal'ko, V. I.; Colombo, L.; Gellert, P. R.; Schwab, M. G.; Kim, K. A roadmap for graphene. *Nature* **2012**, *490*, 192−200.
(2) Dean, C. R.; Wang, L.; Maher, P.; Forsythe, C.; Ghahari, F.; Gao, Y.; Katoch, J.; Ishigami, M.; Moon, P.; Koshino, M.; Taniguchi, T.; Watanabe, K.; Shepard, K. L.; Hone, J.; Kim, P. Hofstadter's Butterfly and The Fractal Quantum Hall Effect in Moiré Superlattices. *Nature* **2013**, *497*, 598−602.
(3) Bandurin, D.-A.; Svintsov, D.; Gayduchenko, I.; Xu, S-G.; Principi, A.; Moskotin, M.; Tretyakov, I.; Yagodkin, D.; Zhukov, S.; Taniguchi, T.; Watanabe, K.; Grigorieva, I.-V.; Polini, M.; Goltsman, G.-N.; Geim, A.-K.; Fedorov, G. Resonant Terahertz Detection using Graphene Plasmons. *Nat. Commun.* **2018**, *9*, No. 5392.
(4) Withers, F.; Del Pozo-Zaumdio, O.; Mishchenko, A.; Rooney, A. P.; Gholinia, A.; Watanabe, K.; Taniguchi, T.; Haigh, S. J.; Geim, A. K.; Tarakovskii, A. I.; Novoselov, K. S. Light-emitting diodes by band-structure engineering in van der Waals heterostructures. *Nat. Mater.* **2015**, *14*, 301−306.
(5) Hong, A. J.; Song, E. B.; Yu, H. S.; Allen, M. J.; Kim, J.; Fowler, J. D.; Wassei, J. K.; Park, Y.; Wang, Y.; Zou, J.; Kaner, R. B.; Weiller, B. H.; Wang, K. L. Graphene Flash Memory. *ACS Nano* **2011**, *5*, 7812−7817.
(6) Moon, J. Y.; Kim, M.; Kim, S. I.; Xu, S.; Choi, J. H.; Whang, D.; Watanabe, K.; Taniguchi, T.; Park, D. S.; Seo, J.; Cho, S. H.; Son, S. K.; Lee, J. H. Layer-engineered large-area exfoliation of graphene. *Sci. Adv.* **2020**, *6*, No. eabc6601.
(7) Some, S.; Kim, J.; Lee, K.; Kulkarni, A.; Yoon, Y.; Lee, S.; Kim, T.; Lee, H. Highly Air-Stable Phosphorus-Doped n-Type Graphene Field-Effect Transistors. *Adv. Mater.* **2012**, *24*, 5481−5486.
(8) Alexandrou, K.; Petrone, N.; Hone, J.; Kymissis, I. Encapsulated Graphene Field-Effect Transistors for Air Stable Operation. *Appl. Phys. Lett.* **2015**, *106*, No. 113104.
(9) Hayasaka, T.; Kubota, Y.; Liu, Y.; Lin, L. The Influences of Temperature, Humidity, and O_2 on Electrical Properties of Graphene FETs. *Sens. Actuators, B* **2019**, *285*, 116−122.
(10) Calizo, I.; Teweldebrhan, D.; Bao, W.; Miao, F.; Lau, C. N.; Balandin, A. A. Spectroscopic Raman Nanometrology of Graphene and Graphene Multilayers on Arbitrary Substrates. *J. Phys.: Conf. Ser.* **2008**, *109*, No. 012008.
(11) Nagashio, K.; Yamashita, T.; Nishimura, T.; Kita, K.; Toriumi, A. Electrical Transport Properties of Graphene on SiO_2 with Specific Surface Structures. *J. Appl. Phys.* **2011**, *110*, No. 024513.
(12) Entani, S.; Takizawa, M.; Li, S.; Naramoto, H.; Sakai, S. Growth of Graphene on SiO_2 with Hexagonal Boron Nitride Buffer Layer. *Appl. Surf. Sci.* **2019**, *475*, 6−11.
(13) Logoteta, D.; Fiori, G.; Lannaccone, G. Graphene-Based Lateral Heterostructure Transistors Exhibits Better Intrinsic Performance than Graphene-Based Vertical Transistors as Post-CMOS Devices. *Sci. Rep.* **2014**, *4*, No. 6607.
(14) Liu, J.-j.; Li, R.; Li, Y.; Li, H.; Yi, J.; Wang, H.; Zhao, X.; Liu, P.; Guo, J.; Liu, L. Graphene-Based in-Plane Heterostructures for Atomically Thin Electronics. *New Carbon Mater.* **2018**, *33*, 481.
(15) Zhang, Z.; Lin, P.; Liao, Q.; Kang, Z.; Si, H.; Zhang, Y. Graphene-Based Mixed-Dimensional Van Der Waals Heterostructures for Advanced Optoelectronics. *Adv. Mater.* **2019**, *31*, No. 1806411.
(16) Kim, T.; Fan, S.; Lee, S.; Joo, M.-J.; Lee, Y. H. High-Mobility Junction Field-Effect Transistor via Graphene/MoS_2 Heterointerface. *Sci. Rep.* **2020**, *10*, No. 13101.
(17) Low, C. G.; Zhang, Q.; Hao, Y.; Ruoff, R. S. Graphene Field Effect Transistors with Mica as Gate Dielectric Layers. *Small* **2014**, *10*, 4213.
(18) Dean, C. R.; Young, A. F.; Meric, I.; Lee, C.; Wang, L.; Sorgenfrei, S.; Watanabe, K.; Taniguchi, T.; Kim, P.; Shepard, K. L.; Hone, J. Boron Nitride Substrates for High Quality Graphene Electronics. *Nat. Nanotechnol.* **2010**, *5*, 722−726.
(19) Laturia, A.; Van de Put, M. L.; Vandenberghe, W. G. Dielectric properties of hexagonal boron nitride and transition metal dichalcogenides: from monolayer to bulk. *npj 2D Mater. Appl.* **2018**, *2*, 6.
(20) Illarionov, Y. Y.; Knobloch, T.; Jech, M.; Lanza, M.; Akinwande, D.; Vexler, M. I.; Mueller, T.; Lemme, M. C.; Fiori, G.; Schwierz, F.; Grasser, T. Insulator for 2D nanoelectronics: The Gap to Bridge. *Nat. Commun.* **2020**, *11*, No. 3385.
(21) Zhang, J.; Tan, B.; Zhang, X.; Gao, F.; Hu, Y.; Wang, L.; Duan, X.; Yang, Z.; Hu, P. Atomically Thin Hexagonal Boron Nitride and its Heterostructures. *Adv. Mater.* **2020**, *33*, 2000769.
(22) Jeong, H.; Kim, D. Y.; Kim, J.; Moon, S.; Han, N.; Lee, S. H.; Okello, O. F. N.; Song, K.; Choi, S.-Y.; Kim, J. K. Wafer-Scale and Selective-Area Growth of High-Quality Hexagonal Boron Nitride on Ni (111) by Metal-Organic Chemical Vapor Deposition. *Sci. Rep.* **2019**, *9*, No. 5736.
(23) Oh, H.; Jo, J.; Tchoe, Y.; Yoon, H.; Lee, H. H.; Kim, S.-S.; Kim, M.; Sohn, B.-H.; Yi, G.-C. Centimeter-Sized Epitaxial h-BN Films. *NPG Asia Mater.* **2016**, *8*, No. e330.
(24) Song, L.; Ci, L.; Lu, H.; Sorokin, P. B.; Jin, C.; Ni, J.; Kvashnin, A. G.; Kvashnin, D. G.; Lou, J.; Yakobson, B. I.; Ajayan, P. M. Large Scale Growth and Characterization of Atomic Hexagonal Boron Nitride layers. *Nano Lett.* **2010**, *10*, 3209−3215.
(25) Shivayogimath, A.; Whelan, P. R.; Mackenzie, D. M. A.; Luo, B.; Huang, D.; Luo, D.; Wang, M.; Gammelgaard, L.; Shi, H.; Ruoff, R. S.; Bøggild, P.; Booth, T. J. Do-It-Yourself Transfer of Large-Area Graphene using An Office Laminator and Water. *Chem. Mater.* **2019**, *31*, 2328−2336.
(26) Glavin, N. R.; Waite, A. R.; Muratore, C.; Bultman, J. E.; Hu, J.; Gengler, J. J.; Voevodin, A. A.; Fisher, T. S. Thermal Conductance at Nanoscale Amorphous Boron Nitride/Metal Interfaces. *Surf. Coat. Tech.* **2020**, *397*, No. 126017.
(27) Zedlitz, R.; Heintze, M.; Schubert, M. B. Properties of Amorphous Boron Nitride Thin Films. *J. Non-Cryst. Solids* **1996**, *198*−*200*, 403−406.
(28) Hong, S.; Lee, C.-S.; Lee, M.-H.; Lee, Y.; Ma, K. Y.; Kim, G.; Yoon, S. I.; Ihm, K.; Kim, K.-J.; Shin, T. J.; Kim, S. W.; Jeon, E.; Jeon, H.; Kim, J.-Y.; Lee, H.-I.; Lee, Z.; Antidormi, A.; Roche, S.; Chhowalla, M.; Shin, H.-J.; Shin, H. S. Ultralow-Dielectric-Constant Amorphous Boron Nitride. *Nature* **2020**, *582*, 511−514.
(29) Glavin, N. R.; Muratore, C.; Jespersen, M. L.; Hu, J.; Hagerty, P. T.; Hilton, A. M.; Blake, A. T.; Grabowski, C. A.; Durstock, M. F.; McConney, M. E.; Hilgefort, D. M.; Fisher, T. S.; Voevodin, A. A. Amorphous Boron Nitride: A Universal, Ultrathin Dielectric for 2D Nanoelectronics. *Adv. Funct. Mater.* **2016**, *26*, 2640−2647.
(30) Uddin, M. A.; Glavin, N.; Singh, A.; Naguy, R.; Jespersen, M.; Voevodin, A.; Koley, G. Mobility Enhancement in Graphene

https://doi.org/10.1021/acsami.2c18706
ACS Appl. Mater. Interfaces 2023, 15, 7274−7281

Transistors on Low Temperature Pulsed Laser Deposited Boron Nitride. *Appl. Phys. Lett.* **2015**, *107*, No. 203110.
(31) Lu, Z.; Zhu, M.; Liu, Y.; Zhang, G.; Tan, Z.; Li, X.; Xu, S.; Wang, L.; Dou, R.; Wang, B.; Yao, Y.; Zhang, Z.; Dong, J.; Cheng, Z.; Chen, S. Low-Temperature Synthesis of Boron Nitride as a Large-Scale Passivation and Protection Layer for Two-Dimensional Materials and High-Performance Devices. *ACS Appl. Mater. Interfaces* **2022**, *14*, 25984−25992.
(32) Lee, J.-H.; Lee, E. K.; Joo, W.-J.; Jang, Y.; Kim, B.-S.; Lim, J. Y.; Choi, S.-H.; Ahn, S. J.; Ahn, J. R.; Park, M.-H.; Yang, C. -W.; Choi, B. L.; Hwang, S.-W.; Whang, D. Wafer-Scale Growth of Single-Crystal Monolayer Graphene on Reusable Hydrogen-Terminated Germanium. *Science* **2014**, *344*, 286−289.
(33) Bresnehan, M. S.; Hollander, M. J.; Wetherington, M.; Wang, K.; Miyagi, T.; Pastir, G.; Snyder, D. W.; Gengler, J. J.; Voevodin, A. A.; Mitchel, W. C.; Robison, J. A. Prospects of Direct Growth Boron Nitride Films as Substrates for Graphene Electronics. *J. Mater. Res.* **2014**, *29*, 459−471.
(34) Liu, N.; Huang, X.; Dubowski, J. J. Selective Area in Situ Conversion of Si (001) Hydrophobic to Hydrophilic Surface by Excimer Laser Irradiation in Hydrogen Peroxide. *J. Phys. D: Appl. Phys.* **2014**, *47*, 385106.
(35) Abbas, Q.; Liang, H.; Shi, J.; Chen, Y.; Xia, X.; Ahmad, A.; Liu, J.; Du, G. Growth and Characterization of Amorphous Boron Nitride Dielectric Films on Si via RF Sputtering at Room Temperature. *Mater. Lett.* **2018**, *227*, 284−288.
(36) Zhao, S.; Zhou, F.; Li, Z.; Liu, H. Effect of Precursor Purity and Flow Rate on The CVD Growth of Hexagonal Boron Nitride. *J. Alloy. Compd.* **2016**, *688*, 1006−1012.
(37) Kutsay, O.; Yan, C.; Chong, Y. M.; Ye, Q.; Bello, I.; Zhang, W. J.; Zapien, J. A.; Zhou, Z. F.; Li, Y. K.; Garashchenko, V.; Gontar, A. G.; Novikov, N. V.; Lee, S. T. Studying Cubic Boron Nitride by Raman and Infrared Spectroscopies. *Diam. Relat. Mater.* **2010**, *19*, 968−971.
(38) Couto, N. J. G.; Costanzo, D.; Engels, S.; Ki, D.-K.; Watanabe, K.; Taniguchi, T.; Stampfer, C.; Guinea, F.; Morpurgo, A. F. Random Strain Fluctuations as Dominant Disorder Source for High-Quality on Substrate Graphene Devices. *Phys. Rev. X* **2014**, *4*, No. 041019.
(39) Lee, J.; Ravichandran, A. V.; Mohan, J.; Cheng, L.; Lucero, A. T.; Zhu, H.; Che, Z.; Catalano, M.; Kim, M. J.; Wallace, R. M.; Venugopal, A.; Choi, W.; Colombo, L.; Kim, J. Atomic Layer Deposition of Boron Nitride for Large-Area 2D Electronics. *ACS Appl. Mater. Interfaces* **2020**, *12*, 36688−36694.
(40) Pandey, H.; Shaygan, M.; Sawallich, S.; Kataria, S.; Wang, Z.; Noculak, A.; Otto, M.; Nagel, M.; Negra, R.; Neumaier, D.; Lemme, M. C. All CVD Boron Nitride Encapsulated Graphene FETs with CMOS Compatible Metal Edge Contacts. *IEEE Trans. Electron Devices* **2018**, *65*, 4129.
(41) Meyer, J. C.; Geim, A. K.; Katsnelson, M. I.; Novoselov, K. S.; Booth, T. J.; Roth, S. The Structure of Suspended Graphene Sheets. *Nature* **2007**, *446*, 60−63.
(42) Yamamoto, M.; Einstein, T. L.; Fuhrer, M. S.; Cullen, W. G. Charge Inhomogeneity Determines Oxidative Reactivity of Graphene on Substrates. *ACS Nano* **2012**, *6*, 8335−8341.
(43) Ferrari, A. C.; Basko, D. M. Raman Spectroscopy as A Versatile Tool for Studying The Properties of Graphene. *Nat. Nanotechnol.* **2013**, *8*, 235−246.
(44) Roscher, S.; Hoffmann, R.; Ambacher, O. Determination of The Graphene-Graphite Ratio of Graphene by Rama 2D Band Symmetry Analysis. *Anal. Methods* **2019**, *11*, 1224−1228.
(45) Gürünlü, B.; Taşdelen-Yücedağ, Ç.; Bayramoğlu, M. One Pot Synthesis of Graphene Through Microwave Assisted Liquid Exfoliation of Graphite in Different Solvents. *Molecules* **2022**, *27*, 5027.
(46) Pantano, M. F.; Iacob, E.; Picciotto, A.; Margesin, B.; Centeno, A.; Zurutuza, A.; Galiotis, C.; Pugno, N. M.; Speranza, G. Investigation of Charges-Driven Interactions Between Graphene and Different SiO_2 Surfaces. *Carbon* **2019**, *148*, 336−343.
(47) Das, A.; Pisana, S.; Chakraborty, B.; Piscanec, S.; Saha, S. K.; Waghmare, U. V.; Novoselov, K. S.; Krishnamurthy, H. R.; Geim, A. K.; Ferrari, A. C.; Sood, A. K. Monitoring Dopants by Raman Scattering in An Electrochemically Top-Gated Graphene Transistor. *Nat. Nanotechnol.* **2008**, *3*, 210−215.
(48) Yao, Y.; Chen, X.; Zhu, J.; Zeng, B.; Wu, Z.; Li, X. The Effect of Ambient Humidity on The Electrical Properties of Graphene Oxide Films. *Nanoscale Res. Lett.* **2012**, *7*, 363.
(49) Ferrari, A. C.; Basko, D. M. Raman Spectroscopy as a Versatile Tool for Studying the Properties of Graphene. *Nat. Nanotechnol.* **2013**, *8*, 235−246.
(50) Lee, Y. G.; Kang, C. G.; Cho, C.; Kim, Y.; Hwang, H. J.; Lee, B. H. Quantitative Analysis of Hysteretic Reactions at The Interface of Graphene and SiO_2 using The Short Pulse I-V Method. *Carbon* **2013**, *60*, 453−460.
(51) Wu, J.-B.; Lin, M.-L.; Cong, X.; Liu, H.-N.; Tan, P.-H. Raman Spectroscopy of Graphene-Based Materials and Its Applications in Related Devices. *Chem. Soc. Rev.* **2018**, *47*, 1822−1873.
(52) Ranjan, A.; Raghavan, N.; O'Shea, S. J.; Mei, S.; Bosman, M.; Shubhakar, K.; Pey, K. L. Conductive Atomic Force Microscope Study of Bipolar and Threshold Resistive Switching in 2D Hexagonal Boron Nitride Films. *Sci. Rep.* **2018**, *8*, No. 2854.
(53) Lee, J.; Ryu, J-H.; Kim, B.; Hussain, F.; Mahata, C.; Sim, E.; Ismail, M.; Abbas, Y.; Abbas, H.; Lee, D-K.; Kim, M-H.; Kim, Y.; Choi, C.; Park, B-G.; Kim, S. Synaptic Characteristics of Amorphous Boron Nitride-Based Memristors on A Highly Doped Silicon Substrate for Neuromorphic Engineering. *ACS Appl. Mater. Interfaces* **2020**, *12*, 33908−33916.
(54) Ra, H.-S.; Lee, A-Y.; Kwak, D.-H.; Jeong, M.-H.; Lee, J.-S. Dual-Gate Black Phosphorus Field-Effect Transistors with Hexagonal Boron Nitride as Dielectric and Passivation Layers. *ACS Appl. Mater. Interfaces* **2018**, *10*, 925−932.
(55) Li, L.; Chung, K.-S.; Jang, J. Field Effect Mobility Model in Organic Thin Film Transistor. *Appl. Phys. Lett.* **2011**, *98*, No. 023305.

https://doi.org/10.1021/acsami.2c18706
ACS Appl. Mater. Interfaces 2023, 15, 7274−7281